Frontal vs. bulk polymerization of fiber-reinforced polymer-matrix composites

S. Vyas[a,c], X. Zhang[a,c,1], E. Goli[b,c], P. H. Geubelle[a,c,2]

[a] *Department of Aerospace Engineering, University of Illinois, Urbana, IL 61801, United States*
[b] *Department of Civil and Environmental Engineering, University of Illinois, Urbana, IL 61801, United States*
[c] *Beckman Institute for Advanced Science and Technology, University of Illinois, Urbana, IL 61801, United States*

Abstract

As frontal polymerization (FP) is being considered as a faster, more energy-efficient, out-of-autoclave manufacturing method for fiber-reinforced thermosetting-polymer-matrix composites (Robertson *et al.*, *Nature*, 2018), the competition between FP and bulk polymerization (BP) is an essential component of the feasibility analysis of the FP-based manufacturing process. To that effect, we present a comparative study of FP and BP based on a nondimensional form of the reaction-diffusion equations that describe the two polymerization processes. From the nondimensional formulation of the thermo-chemical relations, we extract two parameters that involve the key quantities of the cure kinetics model, i.e., the heat of reaction, the time constant, and the activation energy. Although the analysis is general and can be adapted to a wide range of thermosetting-polymer composites, emphasis is placed on unidirectional composites made of carbon or glass fibers embedded in a dicylcopentadiene (DCPD) matrix. The competition between FP and BP is formulated in terms of the

[1] Current address: Department of Mechanical Engineering, University of Wyoming, Laramie, WY, 82071, United States

[2] Corresponding author. Email: geubelle@illinois.edu. Tel: +1(217)244-7648

time scales involved in the two polymerization processes for the manufacturing of composites of varying sizes and fiber volume fraction values.

Keywords:

Frontal polymerization (E), Carbon fibers (A), Glass fibers (A), Polymer-matrix composites (A), Modelling (C).

---

1. Introduction

Traditional manufacturing methods for fiber-reinforced polymer-matrix composites, such as vacuum-assisted resin transfer molding (VARTM) [1], often rely on the bulk polymerization (BP) of the resin in heated molds, ovens or autoclaves, in which the manufactured part is subjected to temperature and pressure cycles [2]. These long and complex cycles are needed to avoid the non-uniform curing of the resin, which can lead to the development of residual stresses [3, 4], and to ensure good quality of the manufactured composite [5]. However, the duration and complexity of these cycles lead to manufacturing processes that are time and energy intensive and produce large amounts of CO_2 [6]. In addition, when assessing the cost of these traditional manufacturing techniques, one must account for the capital investments associated with the need for large heated molds or autoclaves that scale with the size of the manufactured part [7].

In an effort to reduce the cost, duration, and environmental impact of the manufacturing process, Robertson *et al.* [8] recently investigated the feasibility of manufacturing processes for fiber-reinforced composites based on frontal polymerization (FP) of the thermosetting resin. FP [9, 10] is an exothermic reaction process in which a narrow polymerization zone sustained by the heat released during polymerization propagates through the manufactured part. FP has been observed in a variety of thermosetting resins including methacrylic acid [11], epoxies [12, 13] and

dicyclopentadiene (DCPD) [14, 15, 16]. In their experiments, Robertson *et al.* [8] demonstrated the potential of FP-based manufacturing processes by producing high-quality carbon/DCPD composites with mechanical properties that are comparable to those of their oven-cured counterparts. This experimental study was complemented by numerical investigations performed by Goli *et al.* [17] and Vyas *et al.* [18] who adopted a homogenized thermo-chemical relation based on the Prout-Tompkins cure kinetics model [19, 20] to analyze FP in carbon/DCPD and glass/DCPD composites, respectively, with emphasis on extracting the speed, temperature, and width of the propagating front.

The present study builds on this initial work and has two key objectives: (i) to broaden the analysis of the steady-state propagation of the polymerization front to a wider range of resin systems, and, (ii) as BP occurs simultaneously during FP [21], to investigate the competition between FP and BP in terms of the associated time scales involved in the manufacturing process. The analysis is conducted using a nondimensionalized form of the homogenized reaction-diffusion model, from which emerge a characteristic length scale and two key parameters that capture the essence of the impact of the cure kinetics.

The manuscript is organized as follows: The nondimensional form of the coupled reaction-diffusion model describing FP in thermosetting-matrix composites and its conversion to a system of nondimensional coupled ODEs leading to its steady-state solution is summarized in Section 2. The steady-state FP results are presented in Section 3, which summarizes the outcome of a study of the dependence of the front speed on the parameters of the cure kinetics model, the initial temperature of the composite, and the fiber volume fraction. These results are presented both in a nondimensional form for the general case covering a wide range of thermosetting matrices, and in a dimensional form that focuses on the special case of carbon- and

glass-fiber DCPD composites. Section 4 focuses on a comparison of the time scales involved in the FP- and BP-based manufacturing of composites based on the cure kinetics involved and the size of the manufactured component.

2. Frontal polymerization: Reaction-diffusion model

As indicated by Goli *et al.* [17] and Vyas *et al.* [18], FP in DCPD-matrix composites can be described by a coupled thermo-chemical model that combines the thermal diffusion equation for the temperature T (in K) and the phenomenological Prout-Tompkins model for the degree of cure α (nondimensional). In a 1-D setting, these equations take the following form:

$$\begin{cases} \bar{\kappa}\dfrac{\partial^2 T}{\partial x^2} + (1-\phi)\bar{\rho}H_r\dfrac{\partial \alpha}{\partial t} = \bar{\rho}\bar{C_p}\dfrac{\partial T}{\partial t}, \\ \\ \dfrac{\partial \alpha}{\partial t} = Aexp(-\dfrac{E}{RT})(1-\alpha)^n\alpha^m\dfrac{1}{1+exp(c_d(\alpha-\alpha_d))}, \end{cases} \tag{1}$$

where x (in m) is the spatial co-ordinate, t (in s) is the time, $\bar{\kappa}$ (in $W/(m \cdot K)$), $\bar{\rho}$ (in kg/m^3) and $\bar{C_p}$ (in $J/(kg \cdot K)$) respectively denote the homogenized thermal conductivity, density, and heat capacity of the composite, H_r (in J/kg) is the enthalpy of the reaction, A (in $1/s$) is the time constant, E (in J/mol) is the activation energy, R (8.314 $J/(mol \cdot K)$) is the universal gas constant, ϕ is the fiber volume fraction, n and m are the two exponents that define the order of the reaction in the Prout-Tompkins model, while c_d and α_d are the two nondimensional constants introduced to include the effects of diffusion [22]. The material properties denoted by the overbar and entering Eq. (1) are homogenized in the direction of the fibers using the following expression:

$$\bar{(.)} = (.)_m(1-\phi) + (.)_f\ \phi, \tag{2}$$

where the subscripts m and f respectively denote the matrix and the fibers.

2.1. Nondimensional transient formulation

The transient reaction-diffusion relations Eq. (1) can be nondimensionalized by normalizing time, temperature, and the spatial co-ordinate as follows:

$$\tau = At,\ \theta = \frac{T - T_0}{T_{max} - T_0},\ \tilde{x} = \frac{x}{L}, \tag{3}$$

where T_0 is the initial temperature of the composite, T_{max} denotes the maximum temperature associated with the front assuming all the heat released during polymerization goes towards propagating the front,

$$T_{max} = T_0 + \frac{(1-\phi)H_r}{\bar{C}_p}, \tag{4}$$

and the characteristic length scale L is defined as

$$L = \sqrt{\frac{\bar{\kappa}}{\bar{\rho}A\bar{C}_p}}. \tag{5}$$

The coupled thermo-chemical relations can readily be rewritten in their nondimensional form as

$$\begin{cases} \dfrac{\partial^2\theta}{\partial\tilde{x}^2} + \dfrac{\partial\alpha}{\partial\tau} = \dfrac{\partial\theta}{\partial\tau}, \\ \\ \dfrac{\partial\alpha}{\partial\tau} = exp(-\dfrac{\beta}{\theta+\gamma})g(\alpha), \end{cases} \tag{6}$$

where β, γ and $g(\alpha)$ are given by

$$\beta = \frac{E\bar{C}_p}{R(1-\phi)H_r},\ \gamma = \frac{\bar{C}_p T_0}{(1-\phi)H_r},\ g(\alpha) = (1-\alpha)^n \alpha^m \frac{1}{1+exp(c_d(\alpha-\alpha_d))}. \quad (7)$$

Although the impact of the exponents m and n on the propagation speed of the polymerization front will be briefly discussed in Section 3, the emphasis of this study is placed on the role of the nondimensional parameters β and γ, i.e., we assume that the expression for $g(\alpha)$ is fixed. The method can however be readily expanded for other forms of the function $g(\alpha)$ entering the cure kinetics model. It should also be noted at the onset that both β and γ explicitly depend on the fiber volume fraction ϕ through the $(1-\phi)$ term appearing in the denominator, but also implicitly through the expression of the homogenized specific heat $\bar{C}_p = C_{pm}(1-\phi) + C_{pf}\phi$.

2.2. Steady-state formulation

To extract the steady-state solution to the nondimensional thermo-chemical relations Eq. (6), we convert the system of coupled PDEs to a system of coupled ODEs by defining a co-ordinate $\tilde{y}$ attached to the steadily propagating front as

$$\tilde{y} = \tilde{x} - \tilde{V}\tau, \quad (8)$$

where $\tilde{V}$ is the nondimensional constant velocity of the front related to its dimensional counterpart V by

$$\tilde{V} = \frac{V}{AL}, \quad (9)$$

with $\tilde{x}$, τ and L defined earlier in Eq. (3) and Eq. (5). Rewriting Eq. (6) in terms of $\tilde{y}$ yields

$$\begin{cases} \dfrac{d^2\tilde{\theta}}{d\tilde{y}^2} + \tilde{V}\dfrac{d\tilde{\theta}}{d\tilde{y}} - \tilde{V}\dfrac{d\tilde{\alpha}}{d\tilde{y}} = 0, \\ \\ \dfrac{d\tilde{\alpha}}{d\tilde{y}} = -\dfrac{1}{\tilde{V}} exp(-\dfrac{\beta}{\tilde{\theta}+\gamma}) g(\tilde{\alpha}). \end{cases} \tag{10}$$

The resulting system of coupled ODEs is solved with the aid of the following boundary conditions:

$$\begin{cases} \tilde{\theta}(\tilde{y} = -\infty) = \tilde{\theta}_{max}, \quad \tilde{\theta}(\tilde{y} = \infty) = 0, \\ \\ \dfrac{d\tilde{\theta}}{d\tilde{y}}(\tilde{y} = -\infty) = 0, \qquad \dfrac{d\tilde{\theta}}{d\tilde{y}}(\tilde{y} = \infty) = 0, \\ \\ \tilde{\alpha}(\tilde{y} = -\infty) = 1 - \epsilon, \quad \tilde{\alpha}(\tilde{y} = \infty) = \alpha_0, \end{cases} \tag{11}$$

where $\epsilon \ll 1$ (set hereafter to 0.001), α_0 is the initial degree of cure (set hereafter to 0.01) and $\tilde{\theta}_{max}$ is the value of θ when $T = T_0 + \dfrac{(1-\phi)(1-\alpha_0)H_r}{\bar{C}_p}$. Equations (10) and (11) can readily be solved numerically to obtain the dependence of the spatial variation of the temperature and degree-of-cure solutions in the vicinity of the steadily propagating front and of the nondimensional front velocity $\tilde{V}$ on the parameters β and γ.

3. Frontal polymerization results

In this study, the coupled ODEs described by Eq. (10) are solved numerically using the MATLAB ODE15s function [23], which is based on implicit numerical differentiation formulas and an adaptive step size to integrate stiff ODEs. This solver is combined with an optimizer based on a genetic algorithm and the covariance matrix adaptation evolutionary strategy [24] to determine the optimum solution for

$\tilde{V}$ that satisfies the BCs described by Eq. (11). As indicated earlier, DCPD, which was the resin system adopted in the study that motivated this work [8], serves as the reference matrix material in the choice of function $g(\alpha)$ entering the nondimensional cure kinetics relation, Eq. $(10)_2$. The parameters m, n, c_d, and α_d used in this study are listed in Table 1, together with the values of the time constant A, activation energy E, and heat of reaction H_r of DCPD. Table 2 contains the material properties for DCPD, carbon fibers, and glass fibers used in studies by Goli *et al.* [17] and Vyas *et al.* [18].

n	m	c_d	α_d	A $(\frac{1}{s})$	E $(\frac{kJ}{mol})$	H_r $(\frac{J}{g})$
1.72	0.77	14.48	0.41	$8.55 * 10^{15}$	110.75	350.0

Table 1: Cure kinetics parameters of the Prout-Tompkins model Eq. (1) for DCPD.

	κ $(\frac{W}{m.K})$	ρ $(\frac{kg}{m^3})$	C_p $(\frac{J}{kg.K})$
DCPD	0.15	980.0	1600.0
Carbon fibers	9.363	1800.0	753.6
Glass fibers	1.275	2575.0	802.5

Table 2: Thermal conductivity, density, and specific heat capacity of DCPD, carbon fibers, and glass fibers considered in this study.

Figure 1 presents typical steady-state solution profiles for the temperature and degree of cure with the corresponding solution for the nondimensional front velocity $\tilde{V}$ for two values of the fiber volume fraction ϕ. The corresponding values of the parameters β and γ defined in Eq. (7) are chosen specifically for the case of carbon/DCPD composites, i.e., $\beta = 60.89$ and $\gamma = 1.34$ for the case $\phi = 0\%$, and $\beta = 89.58$ and $\gamma = 1.97$ for the case with $\phi = 50\%$. As expected, the thermal front

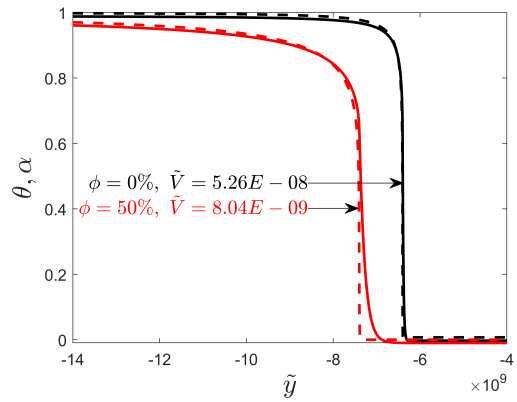

Figure 1: Typical steady-state solution profiles obtained for the nondimensional temperature θ (solid curves) and the degree of cure α (dashed curves) for two values of the fiber volume fraction, $\phi = 0\%$ and 50%, with the corresponding values of the nondimensional front velocity $\tilde{V}$.

precedes the degree-of-cure front. We also note that the front is sharper for the neat resin case ($\phi = 0\%$) than in the composite case ($\phi = 50\%$) due to the increased thermal conductivity associated with the presence of the more conductive carbon fibers.

Expanding on the results shown in Figure 1, we present in Figure 2 the steady-state nondimensional ($\tilde{V}$ - Figure 2a) and dimensional (V in mm/s - Figure 2b) velocities of the polymerization front for every pair of (β, γ) in the vicinity of the values of the two nondimensional parameters corresponding to the neat DCPD resin (denoted by the red dot). As apparent there, faster front propagation is achieved by decreasing β, i.e., by decreasing the activation energy E, and/or by increasing γ, i.e., by increasing the initial temperature T_0 of the resin. The 'almost parallel nature' of the $\tilde{V}$ and V contour lines indicates that the front velocity depends primarily on the ratio $\beta/\gamma = E/RT_0$.

The numerical results shown in Figure 2 can be compared to the following ana-

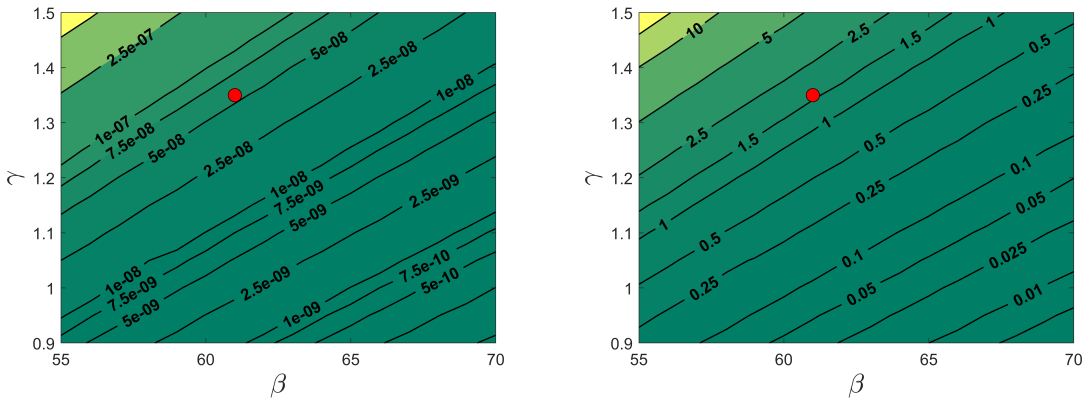

(a) (b)

Figure 2: Nondimensional (a) and dimensional (b) front velocity contours for a portion of the (β, γ) space in the neighborhood of the neat DCPD resin (i.e., $\phi = 0\%$), which is denoted by a red dot.

lytical expression of the front velocity, V_a, derived by Novozhilov [25] and discussed by Garbey *et al.* [26] for the simplified zeroth-order reaction kinetics (i.e., for which $g(\alpha) = 1$ for $\alpha < 1$ and $g(\alpha) = 0$ otherwise):

$$V_a = \sqrt{\frac{2A\kappa}{\rho H_r}\frac{RT_{max}^2}{E}exp(-\frac{E}{RT_{max}})}, \tag{12}$$

where, for the neat resin, $T_{max} = T_0 + \dfrac{H_r}{C_{pm}}$. In terms of the parameters β and γ introduced earlier, this expression can be rewritten in a nondimensional form as

$$\tilde{V}_a = \sqrt{\frac{2}{\beta}(1+\gamma)^2 exp(-\frac{\beta}{1+\gamma})}. \tag{13}$$

Using Eq. (13), we can construct in Figure 3a, a contour plot of $\tilde{V}_a$ in the same (β, γ) space as that used for Figure 2a. As apparent there, the dependence of the front velocity on the two nondimensional parameters β and γ is very similar, although the analytical values exceed their numerical counterparts by about an order of magnitude.

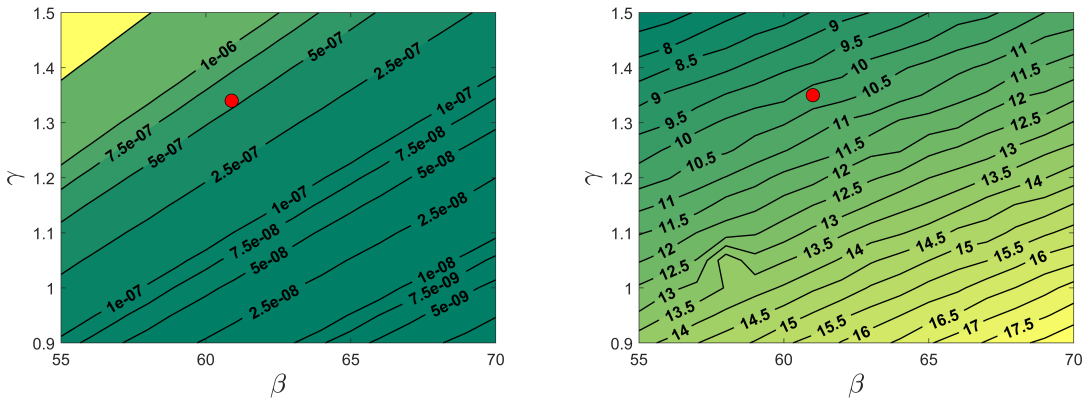

(a) (b)

Figure 3: (a) Nondimensional front velocity contours obtained analytically using Eq. (13) for a portion of the (β, γ) space in the neighborhood of the neat DCPD resin solution ($\phi = 0\%$), which is denoted by the red dot. (b) Ratio between analytical and numerical values of the front velocity.

This difference is likely due to the simplified form of the cure kinetics model adopted in the derivation of V_a. As shown in Figure 3b, the ratio $\tilde{V}_a/\tilde{V}$ varies with both β and γ with the higher discrepancies between analytical and numerical solutions obtained for high values of the activation energy E and low values of the initial temperature T_0.

Turning our attention to composites, we note that the front velocity V is doubly dependent on the fiber volume fraction ϕ through the nondimensional parameters β and γ and the length scale L defined in Eq. (5). We explore this dependency by computing the nondimensional velocity $\tilde{V}$ for values of (β, γ) around those of the carbon/DCPD composite with $\phi = 50\%$ (for which $\beta = 89.58$ and $\gamma = 1.97$). Using Eq. (9), we then convert $\tilde{V}$ to the dimensional velocity V to obtain the contour plot shown in Figure 4a. As L explicitly depends on the homogenized thermal diffusivity $\bar{\kappa}/\bar{\rho}\bar{C}_p$ of the composite and the pre-exponential constant A entering the cure kinetics

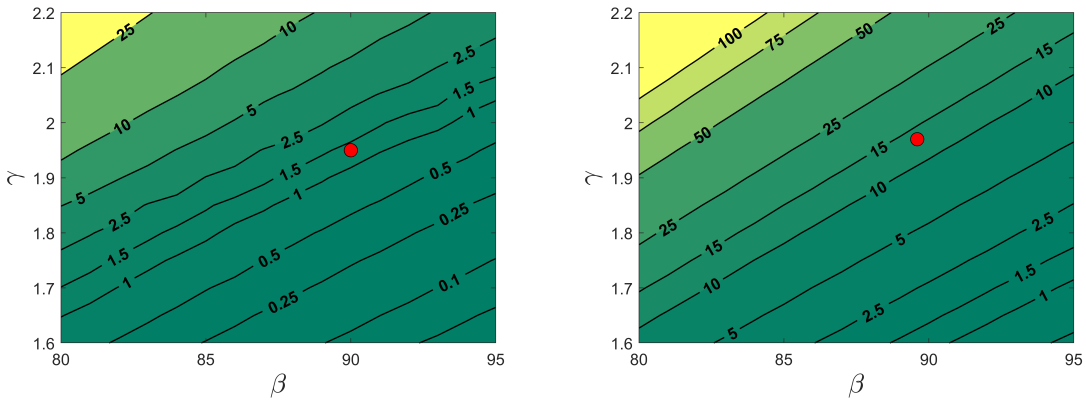

(a) (b)

Figure 4: Numerical (a) and analytical (b) front velocity V contours obtained for a portion of the (β, γ) space in the neighborhood of the reference carbon/DCPD composite with fiber volume fracton $\phi = 50\%$ (denoted by the red rot). As alluded to in Figure 3b, the analytical prediction is an order of magnitude higher than its numerical counterpart.

model, the contours presented in Figure 4 are unique for the reference carbon/DCPD system whose material properties are given in Table 2.

The analytical expression for the front velocity (Eq. (12)) can be modified for the composite case by substituting κ and ρ with their homogenized counterparts (Eq. (2)), replacing H_r with $(1-\phi)H_r$ to account for the reduction in total heat of the reaction associated with the presence of the fibers, and using Eq. (4) for T_{max} as

$$V_a = \sqrt{\frac{2A\bar{\kappa}}{\bar{\rho}(1-\phi)H_r}\frac{RT_{max}^2}{E}exp(-\frac{E}{RT_{max}})}. \tag{14}$$

In its nondimensional form, the above relation conveniently reduces to Eq. (13). The (β, γ) dependence of the analytical expression V_a of the front velocity for the carbon/DCPD composite with $\phi = 50\%$ is presented in Figure 4b. A direct comparison between Figure 4a and Figure 4b shows that, while it captures the essence

of the dependence of the front velocity on β and γ, the analytical expression again overpredicts its numerical counterpart by about an order of magnitude.

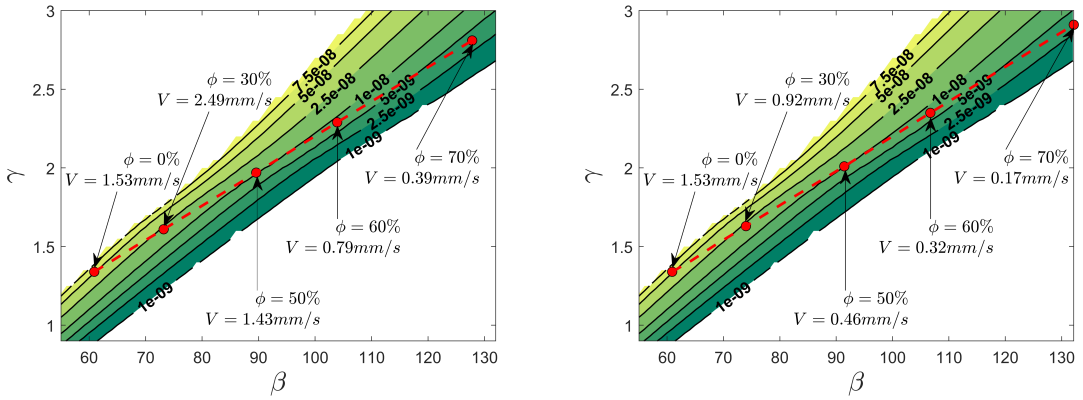

(a) (b)

Figure 5: Contours of $\tilde{V}$ in the (β, γ) space. The dashed curves denote the (β, γ) loci as the fiber volume fraction ranges from 0% to 70% for the case of (a) carbon/DCPD and (b) glass/DCPD composites. Some specific values of ϕ and their corresponding dimensional velocity V values are marked by the red dots.

Figure 5 presents similar contour plots for a wider range of values of β and γ, showing the loci in the (β, γ) space for carbon/DCPD (Figure 5a) and glass/DCPD (Figure 5b) composites with fiber volume fraction values ranging from $\phi = 0\%$ to $\phi = 70\%$. The dimensional values V of the front velocity are also provided for five values of ϕ: 0, 30, 50, 60, and 70%. As shown by Goli *et al.* [17], the front velocity in carbon/DCPD has a non-monotonic dependence on the fiber volume fraction, reaching a maximum for $\phi \simeq 20\%$ before progressively decreasing due to an increasing deficit in resin content as ϕ increases. As pointed out by Vyas *et al.* [18], the lower thermal conductivity of glass leads to a monotonically decreasing dependence of V on ϕ, as shown in Figure 5b.

The results presented thus far have assumed a fixed expression for $g(\alpha)$ defined

in Eq. (7) with the associated parameters listed in Table 1. To assess the impact of the exponents m and n entering the cure kinetics model, we present in Figure 6 front velocity contours in the (m, n) space for the two reference cases showed in Figure 1, while keeping the values for c_d and α_d constant. As apparent there, the sensitivity of the front speed V on m and n is relatively small, with higher front speeds obtained for lower values of the two exponents as decreasing the values on m and n leads to a net increase in the reaction rate.

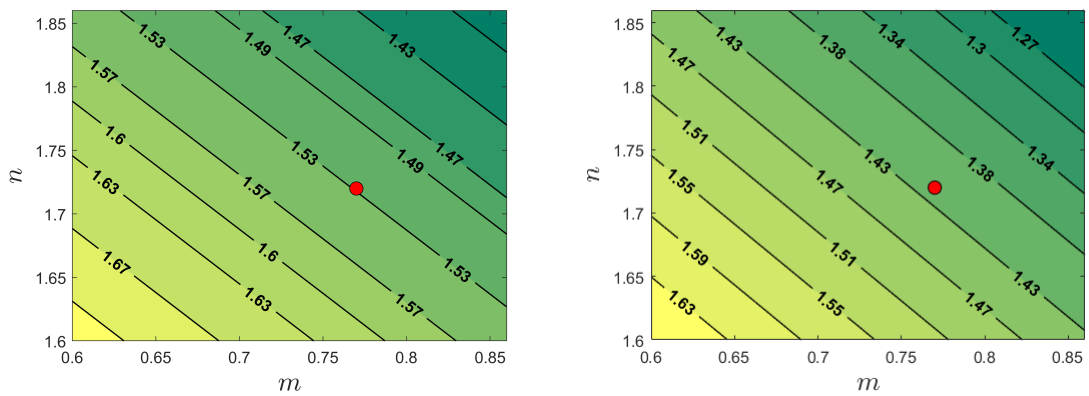

(a) (b)

Figure 6: Front velocity contours (in mm/s) in a portion of the (m, n) space around the reference carbon/DCPD composite case (denoted by the red dot) with fiber volume fraction values $\phi = 0\%$ (a) and $\phi = 50\%$ (b).

4. Frontal polymerization vs. bulk polymerization

One of the key results of the previous section is the existence of a steadily propagating polymerization front for a wide range of values of β and γ. However, for many of these values, the predicted front speed is very small, which makes the FP-based manufacturing of composites impractical. To assess the feasibility of FP-based

manufacturing, one should compare the time scale t_{BP} involved in the bulk polymerization of the resin to that associated with frontal polymerization of a manufactured part of size D,

$$t_{FP} = \frac{D}{V}, \tag{15}$$

which, in its nondimensional form, is given by

$$\tau_{FP} = \frac{D}{L\tilde{V}}. \tag{16}$$

Due to the distributed nature of the bulk polymerization (BP), the time scale associated with BP, t_{BP}, does not depend on the size of the manufactured part, but can be determined by solving Eq. (6) in the absence of the diffusion term:

$$\begin{cases} \dfrac{d\alpha}{d\tau} = \dfrac{d\theta}{d\tau}, \\ \\ \dfrac{d\alpha}{d\tau} = exp(-\dfrac{\beta}{\theta+\gamma})g(\alpha). \end{cases} \tag{17}$$

This system of coupled ODEs can also be readily solved with the aid of MATLAB function ODE15s by setting the initial conditions $\alpha(0) = \alpha_0$ (set at 0.01 as indicated earlier) and $\theta(0) = 0$, yielding evolution curves for the temperature and degree of cure such as those shown in Figure 7. As also illustrated in that figure, the characteristic time scale associated with BP, τ_{BP}, can be extracted as the time value for which $\alpha(\tau_{BP}) = 0.5$. As expected, the characteristic time associated with the bulk polymerization of the composite is higher than that for neat resin due to the factor $(1 - \phi)$ multiplying the heat of reaction H_r in the expression of β and γ in Eq. (7).

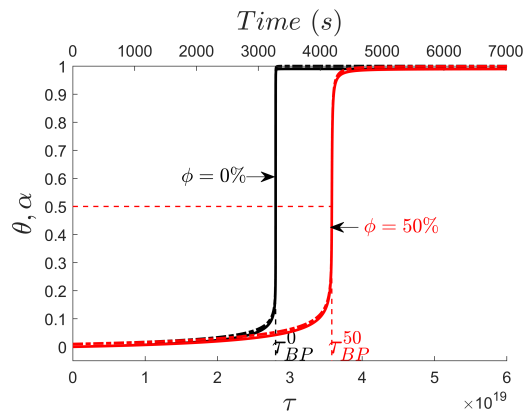

Figure 7: Bulk polymerization: evolution of θ and α obtained by solving Eq. (17) for the carbon/DCPD system with fiber volume fractions $\phi = 0\%$ (black curves) and $\phi = 50\%$ (red curves) and extraction of the characteristic time τ_{BP}.

Based on these definitions of the characteristic time scales, we can describe the competition between FP and BP by revisiting the contour plots of the front velocity V presented earlier in Figure 2b and Figure 4a, and by indicating on those graphs the minimum front speed marking the 'feasibility boundary' between FP- and BP-based manufacturing for a given part size D. The results are presented in Figure 8 for $D = 1m$ and $D = 10m$ for the case of the neat reference DCPD resin (Figure 8a) and reference carbon/DCPD system with $\phi = 50\%$ (Figure 8b). As indicated there, the (β,γ) values located above the reference (thicker) contour line correspond to cases for which $1m$ or $10m$-size parts can be manufactured using FP. Conversely, the area of the (β,γ) domain located below the reference contour denotes conditions for which BP would take place before a polymerization front can propagate the entire length of the manufactured part.

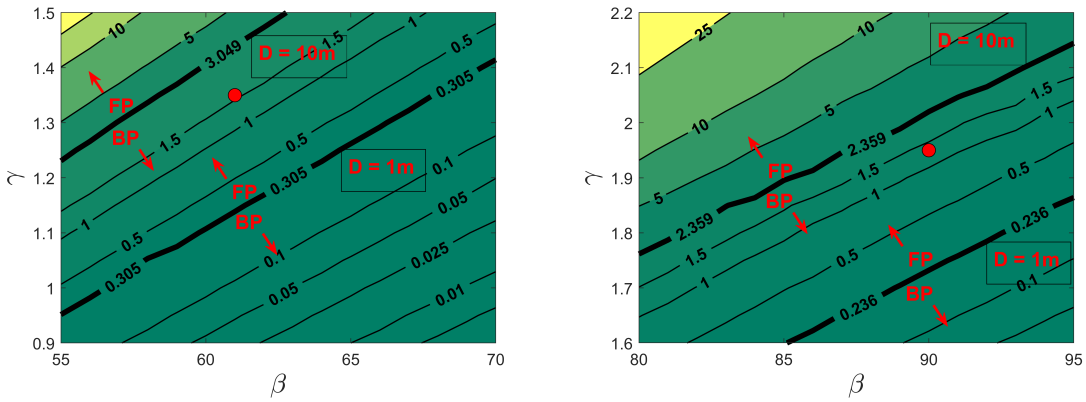

(a) (b)

Figure 8: Competition between FP and BP: Reference contour line of the front velocity V (given in mm/s), with the thicker contour lines marking the feasibility boundary between BP (below) and FP (above) for parts of size $D = 1m$ and $D = 10m$ for the manufacturing of neat resin i.e., $\phi = 0\%$ (a) and $\phi = 50\%$ (b). The red dots correspond to the results for the reference carbon/DCPD system.

5. Conclusion

In this manuscript, we have presented an analytical study of the competition between frontal- and bulk-polymerization-based manufacturing of thermosetting-matrix composites with the aid of a nondimensional form of the reaction-diffusion thermo-chemical equations. After reducing the problem to two key nondimensional parameters and extracting the steady-state solution, we have explored the effects of fiber volume fraction, thermal properties, and cure-kinetics parameters on the velocity of the front for a range of material systems. The time scale involved in the propagation of the polymerization front over the size of the manufactured part was then compared to the time scale associated with the bulk polymerization of the resin, suggesting the existence of a feasibility limit of the FP-based manufacturing of thermosetting-matrix composites.

Acknowledgments

This work was supported by the Air Force Office of Scientific Research through Award FA9550-16-1-0017 (Dr. B. 'Les' Lee, Program Manager) as part of the Center for Excellence in Self-Healing, Regeneration, and Structural Remodeling. This work was also supported by the National Science Foundation (NSF Grant No. 1830635) through the LEAP-HI: Manufacturing USA program. The authors would like to acknowledge Professors Nancy Sottos and Jeffrey Moore for insightful discussions on this work.

References

[1] D. Bender, J. Schuster, D. Heider, Flow rate control during vacuum-assisted resin transfer molding (VARTM) processing, Composites Science and Technology 66 (13) (2006) 2265–2271.

[2] D. Purslow, R. Childs, Autoclave moulding of carbon fibre-reinforced epoxies, Composites 17 (2) (1986) 127–136.

[3] T. Bogetti, J. Gillespie Jr, Process-induced stress and deformation in thick-section thermoset composite laminates, Journal of Composite Materials 26 (5) (1992) 626–660.

[4] K. Tarsha-Kurdi, P. Olivier, Thermoviscoelastic analysis of residual curing stresses and the influence of autoclave pressure on these stresses in carbon/epoxy laminates, Composites Science and Technology 62 (4) (2002) 559–565.

[5] L. Davies, R. Day, D. Bond, A. Nesbitt, J. Ellis, E. Gardon, Effect of cure cycle heat transfer rates on the physical and mechanical properties of an epoxy matrix composite, Composites Science and Technology 67 (9) (2007) 1892–1899.

[6] A. Timmis, A. Hodzic, L. Koh, M. Bonner, C. Soutis, A. Schäfer, L. Dray, Environmental impact assessment of aviation emission reduction through the implementation of composite materials, The International Journal of Life Cycle Assessment 20 (2) (2015) 233–243.

[7] D. Abliz, Y. Duan, L. Steuernagel, L. Xie, D. Li, G. Ziegmann, Curing methods for advanced polymer composites-a review, Polymers and Polymer Composites 21 (6) (2013) 341–348.

[8] I. Robertson, M. Yourdkhani, P. Centellas, J. Aw, D. Ivanoff, E. Goli, E. Lloyd, L. Dean, N. Sottos, P. Geubelle, J. Moore, S. White, Rapid energy-efficient manufacturing of polymers and composites via frontal polymerization, Nature 557 (7704) (2018) 223.

[9] J. Pojman, V. Ilyashenko, A. Khan, Free-radical frontal polymerization: self-propagating thermal reaction waves, Journal of the Chemical Society, Faraday Transactions 92 (16) (1996) 2825–2837.

[10] D. Fortenberry, J. Pojman, Solvent-free synthesis of polyacrylamide by frontal polymerization, Journal of Polymer Science Part A: Polymer Chemistry 38 (7) (2000) 1129–1135.

[11] S. Solovyov, V. Ilyashenko, J. Pojman, Numerical modeling of self-propagating polymerization fronts: The role of kinetics on front stability, Chaos: An Interdisciplinary Journal of Nonlinear Science 7 (2) (1997) 331–340.

[12] A. Mariani, S. Bidali, S. Fiori, M. Sangermano, G. Malucelli, R. Bongiovanni, A. Priola, Uv-ignited frontal polymerization of an epoxy resin, Journal of Polymer Science Part A: Polymer Chemistry 42 (9) (2004) 2066–2072.

[13] E. Frulloni, M. Salinas, L. Torre, A. Mariani, J. Kenny, Numerical modeling and experimental study of the frontal polymerization of the diglycidyl ether of bisphenol a/diethylenetriamine epoxy system, Journal of Applied Polymer Science 96 (5) (2005) 1756–1766.

[14] I. Robertson, E. Pruitt, J. Moore, Frontal ring-opening metathesis polymerization of exo-dicyclopentadiene for low catalyst loadings, ACS Macro Letters 5 (5) (2016) 593–596.

[15] A. Ruiu, D. Sanna, V. Alzari, D. Nuvoli, A. Mariani, Advances in the frontal ring opening metathesis polymerization of dicyclopentadiene, Journal of Polymer Science Part A: Polymer Chemistry 52 (19) (2014) 2776–2780.

[16] A. Mariani, S. Fiori, Y. Chekanov, J. Pojman, Frontal ring-opening metathesis polymerization of dicyclopentadiene, Macromolecules 34 (19) (2001) 6539–6541.

[17] E. Goli, N. Parikh, M. Yourdkhani, N. Hibbard, J. Moore, N. Sottos, P. Geubelle, Frontal polymerization of unidirectional carbon-fiber-reinforced composites, Composites Part A: Applied Science and Manufacturing (2019) 105689.

[18] S. Vyas, E. Goli, X. Zhang, P. Geubelle, Manufacturing of unidirectional glass-fiber-reinforced composites via frontal polymerization: A numerical study, Composites Science and Technology (2019) 107832.

[19] M. Kessler, S. White, Cure kinetics of the ring-opening metathesis polymerization of dicyclopentadiene, Journal of Polymer Science Part A: Polymer Chemistry 40 (14) (2002) 2373–2383.

[20] E. Goli, I. Robertson, P. Geubelle, J. Moore, Frontal polymerization of dicyclopentadiene: A numerical study, The Journal of Physical Chemistry B 122 (16) (2018) 4583–4591.

[21] S. Cardarelli, D. Golovaty, L. Gross, V. Gyrya, J. Zhu, A numerical study of one-step models of polymerization: Frontal versus bulk mode, Physica D: Nonlinear Phenomena 206 (3-4) (2005) 145–165.

[22] G. Yang, J. Lee, Curing kinetics and mechanical properties of endo-dicyclopentadiene synthesized using different Grubbs' catalysts, Industrial & Engineering Chemistry Research 53 (8) (2014) 3001–3011.

[23] L. Shampine, M. Reichelt, The MATLAB ODE suite, SIAM Journal on Scientific Computing 18 (1) (1997) 1–22.

[24] N. Hansen, A. Ostermeier, Adapting arbitrary normal mutation distributions in evolution strategies: The covariance matrix adaptation, in: Proceedings of IEEE International Conference on Evolutionary Computation, IEEE, 1996, pp. 312–317.

[25] B. Novozhilov, Propagation rate of the front of an exothermic reaction in condensed phase, in: Proceedings of Doklady Akademii Nauk, Vol. 141, Russian Academy of Sciences, 1961, pp. 151–153.

[26] M. Garbey, A. Taik, V. Volpert, Linear stability analysis of reaction fronts in liquids, Quarterly of Applied Mathematics 54 (2) (1996) 225–247.